M -plane AlGaN digital alloy for microwire UV-B LEDs

Lucie Valera, Vincent Grenier, Sylvain Finot, C. Bougerol, Joël Eymery, Gwénolé Jacopin, Christophe Durand

M-plane AlGaN digital alloy for microwire UV-B LEDs

Lucie Valera[1,2], Vincent Grenier[1], Sylvain Finot[2], Catherine Bougerol[2], Joël Eymery[3], Gwénolé Jacopin[2], Christophe Durand[1,a)]

[1] *Univ. Grenoble Alpes, CEA, IRIG, PHELIQS, NPSC, 38000 Grenoble, France*

[2] *Univ. Grenoble Alpes, CNRS, Grenoble INP, Institut Néel, 38000 Grenoble, France*

[3] *Univ. Grenoble Alpes, CEA, IRIG, MEM, NRS, 38000 Grenoble, France*

a) Author to whom correspondence should be addressed*: christophe.durand@cea.fr*

Keywords: AlGaN, digital alloys, LED, core-shell microwires, MOVPE

Abstract

The growth of non-polar AlGaN digital alloy (DA) is achieved by metal-organic vapor phase epitaxy using GaN microwire m-facets as the template. This AlGaN DA consisting in 5 periods of 2 monolayers-thick layers of GaN and AlGaN (approximately 50% Al-content) is integrated into the middle of an n-p GaN/AlGaN junction to design core-shell wire-µLED. The optical emission of the active zone investigated by 5 K cathodoluminescence is consistent with the AlGaN bulk alloy behavior. Several contributions from 295 to 310 nm are attributed to the lesser thickness and/or composition fluctuations of AlGaN DA. Single-wire µLED is fabricated using a lithography process and I-V measurements confirms a diode rectifying behavior. Room temperature UV electroluminescence originating from m-plane AlGaN DA is accomplished at 310 nm.

Nowadays, AlGaN-based LEDs represent an eco-friendly substitute to current mercury-based lamp UV sources, well-known to be hazardous for people and environment. Although significant development of UV-LEDs, these devices still suffer from poor efficiency. Within this framework, many innovative approaches are explored in order to overcome this efficiency limitation. In this context, short period GaN/AlN superlattices involving sub-4 monolayers (ML) for GaN or AlN layers have been the subject of interest in recent years.[1,2] At this kind of thickness the wavefunctions are completely delocalized in the layer without any confinement effect which leads to similar properties as random distributed AlGaN alloys. This kind of ordered alloy forming superlattices is called "digital alloy" (DA) and noted $(GaN)_n/(AlN)_m$ with *n* and *m* referring to the number of GaN and AlN MLs respectively.[1,3]

Spontaneous formation of AlGaN DA have been reported in the literature for samples grown using molecular beam epitaxy (MBE).[2] The origin of this phenomenon is strongly dependent on the growth conditions (kinetics) and also related to minimization of the total energy (thermodynamics).[4,5] Unfortunately, this form of spontaneous DA AlGaN is difficult to integrate into devices due to growth control issues and intentional DA heterostructures have therefore been preferred.[6]

Moreover, the spontaneous formation of AlGaN DAs has been reported for samples grown using metal-organic vapor phase epitaxy (MOVPE).[7] The same growth control and reproducibility concerns have led to DA intentionally being grown while managing additional difficulties to achieve ML-scale growth using the MOVPE technique.[8] ML-scale growth can be achieved by the development of delayed sequential growth process to assure sharp interfaces.[9]

Based on these studies, intentionally ordered AlGaN DA have been grown to take advantage of their ordered characteristics to address electronic and transport issues for diverse applications.[6,9–12] Resonant electron tunneling in an AlGaN-based heterostructure is mandatory for cascade lasers or high-speed electronic oscillators applications and has been improved by replacing the AlGaN barrier by AlGaN DA.[11] Also, enhanced unipolar vertical transport has been predicted by suppressing the random alloy fluctuations of AlGaN barriers in GaN/AlGaN heterostructures.[10]

The use of AlGaN DAs is also one of the paths explored to target efficient UV LEDs. Indeed, efforts have been made in recent years to address recurring issues of UV LEDs, as the emitted light extraction issue or the poor p-doping of AlGaN-based materials due to high activation energy of Mg dopants.[13–18] In this context, highly doped DAs has been developed to perform ohmic contacts, taking advantage of the lower activation energy of dopants in GaN. [12,19,20] In the literature, the AlGaN DA formation in spontaneous or controlled growth mode has been studied for standard c-oriented surfaces but few groups have reported on semi-polar or non-polar AlGaN DA and those that have only worked on spontaneous formation.[4,7,21] However, non-polar surfaces offer an alternative to c-plane growth for future UV-LEDs with enhanced recombination rate and no quantum confined Stark effect.[22–24] Recently, non-polar UV emitters have been developed using lithography-free AlN nanorods[25], hybrid top down/bottom-up process for AlN nanorods growth[26,27], non-polar AlGaN microfins[28], InAlN-based microtubes[29] or dislocation-free GaN nano/microwires[30–32] to overcome the high cost of non-polar substrates. Focusing on GaN wire-based technology, UV µLEDs have recently achieved core-shell electroluminescence emission ranging from UV-A to UV-B.[32,33] In this context, the growth of non-polar AlGaN DA is one of the mandatory steps to continue the current development efforts of non-polar UV-LEDs.

In this work, AlGaN DA was intentionally grown on the *m*-plane facets of GaN microwires. Room-temperature core-shell UV emission from DA was achieved at 310 nm, enabling the production of single-wire µLEDs.

N-polar GaN microwires were grown spontaneously on c-sapphire using a closed coupled showerhead (3x2'') MOVPE reactor. A 2 nm thick annealed SiN_x layer previously formed on the sapphire surface provided preferential nucleation points for the GaN growth. GaN microwires were grown at 800 mbar and 1040°C using a silane-assisted process and a low V/III ratio (≃ 50) to promote vertical growth.[34] The precursors used for microwires growth were TMGa, NH_3 and SiH_4 with respective fluxes of 135 µmol.min^{-1}, 2 232 µmol.min^{-1} and 200 nmol.min^{-1}. High SiH_4 flux led to the formation of SiN_x passivation layer on the m-surface of the microwire and produced ~10^{20} at./cm^3 n-dopant concentration.[35] After 700 s, the silane flux was switched off and the GaN microwire growth continued for another 600s with n-dopant concentration of ~10^{19} at. /cm^3.[36] Because of the selectivity between GaN and SiN_x, the shell growth only occurs at the silane-free upper part of GaN microwires. Once the GaN microwire finished, the UV LED shell with embedded AlGaN DA n-i-p heterostructure was grown following the stack illustrated in Fig.1. Non-intentionally doped GaN shell was grown at 920°C and 150 mbar using NH_3 (66.9 mmol.min^{-1}) and TMGa (24.8 µmol.min^{-1}) to bury a thin SiGaN layer formed by silane residues and to prevent the formation of extended defects.[37] TMGa precursor was then switched by TEGa to perform a GaN buffer growth at ~3.6 µmol.min^{-1}. First 20 nm n-doped AlGaN graduated composition layer (0-30 % Al-content) was grown to address the strain management issue using 3.6, 0-3.65, 66 900 and 0.012 µmol. min^{-1} for TEGa, TMAl, NH_3 and SiH_4.[38,39] N-doped $Al_{30}Ga_{70}N$ cladding layer of 10 nm was then grown. For 600 s, the TMAl flux was linearly increased from 3.6 to 7.2 µmol.min^{-1} to grow a second 20 nm gradual AlGaN n-doped layer from 30 to 60% Al composition. The precursors' fluxes are

preserved to grow the AlGaN DA active area, which is composed of 5x (GaN/AlGaN) with an Al-content of approximately 50% in AlGaN. Both low precursor flux and brief growth time (40 s for GaN, 15 s for AlGaN) were used to produce a ML-scale like growth. Then, a 8 nm p-doped AlGaN linear gradient layer varying the Al composition from 60 to 30 % was grown using 0.3 µmol.min^{-1} Cp_2Mg flux, followed by 10 nm p-doped $Al_{0.3}Ga_{0.7}N$ layer. A p-GaN shell of 33 nm was then grown using 45, 178 000 and 0.7 µmol.min^{-1} flows of TMGa, NH_3 and Cp_2Mg. Finally, a p^+-GaN layer was grown using 0.8 and 34 µmol.min^{-1} of Cp_2Mg and TMGa to ensure ohmic contact. The p-doping was later activated by annealing under N_2 atmosphere at 700°C for 20 min.

To characterize the structural properties of the core-shell growth, we carried out scanning Transmission Electron Microscopy (STEM) observations using a high-angle annular dark field detector (HAADF) on a FEI-Technai microscope operated at 200 kV with a thin longitudinal cross-section slice of the wires prepared using a focused ion beam (FIB). Figure 2a) shows the STEM-HAADF image performed along the *a*-zone axis on the upper part of a microwire cross-section. The HAADF contrast reveals the presence of a homogeneous Al-rich shell growth all along the wire (bright contrast). The presence of deep cracks in a transversal direction was also observed propagating towards the GaN core of the microwire (linear density about 2 cracks/µm) (see Supporting information S1). Their formation has already been reported for Al-rich shells[30,38] and it has been well established that strain relaxation occurs through the formation of cracks, in a similar way to the AlGaN planar growth on GaN templates.[40] Figure 2b) presents a high resolution image of the active zone obtained in off-axis TEM mode (10° off-axis from the [11-20] zone axis). In Figure 2b) corresponding to an enlargement of the core-shell LED structures, the growth of 18 nm-thick p-AlGaN followed by 33 nm-thick p-GaN shell is observed. A zoom-in focused on the active zone, illustrated in Figures 2c) and 2d) reveals

the ML-heterostructure, consisting in 5 periods of 2 dark MLs followed by 2 bright MLs attributed to the growth of 5 nm-thick AlGaN DA composed as follows: $(GaN)_2/(AlGaN)_2$. It is remarkable to notice in Figure 2c) that the $(GaN)_2/(AlGaN)_2$ DA is maintained along the *m*-plane sidewall facets of the microwire. Additional HR-TEM observations reveal that the DA structure is also maintained near crack (see Supporting information S2). Since the thickness of the DA stay invariant along sidewalls whatever wire diameter, the DA growth is mainly driven by the gas phase. Local variations within the ±2 ML range can be observed either for GaN or AlGaN. Also, we cannot exclude any local variation of Al-content composition at the ML scale and Al residue in the GaN layers. These TEM analyses definitely evidence the achievement of AlGaN DA in the form of $(GaN)_2/(AlGaN)_2$ and located at the middle of the n-p AlGaN/GaN junction.

Cathodoluminescence (CL) measurements were then performed based on field emission gun (FEG)-SEM with an embedded helium cryostat. A charged-coupled device (CCD) with monochromator analyzed the CL signals collected by parabolic mirror from a typical single microwire, which was mechanically dispersed onto a silicon substrate. Spot mode (effective interaction volume is estimated about 200 nm) was used to characterize the DA optical emission and each spot position taken along the microwire is highlighted with rainbow-like colored dots on Figure 3a). The corresponding normalized spectra measured at 5K with 5kV acceleration voltage are depicted in Figure 3b). Core-shell UV emission from the AlGaN DA is demonstrated with full width at half maximum between 5 to 10 nm exhibiting a stronger intensity at the upper part of the microwire. The decreasing CL intensity moving down the wire can be attributed to a better crystal growth of AlGaN DA near the top part. The broad shape of spectra at 5K is consistent with an emission from AlGaN alloy.[41] The CL spectra are composed of multiple contributions centered around 300 nm which correspond

approximately to $Al_{0.27}Ga_{0.73}N$ bulk emission.[41] Eleven contributions with various intensity from 296 nm to 307 nm can be identified taking all spectra (highlighted by arrows and dotted lines in Figure 2b)) into account. These contributions cannot be simply attributed to the presence of localization centers for DA. In the case of $(GaN)_n/(Al_xGa_{1-x}N)_m$ DA, the equivalent Al composition considering a bulk $Al_yGa_{1-y}N$ alloy was estimated following the formula :

$$y = \frac{M_{AlGaN}}{M_{AlGaN} + N_{GaN}} x$$

where M_{AlGaN} and N_{GaN} represent respectively the total number of ML of AlGaN and GaN in the full thickness of AlGaN DA superlattice. Each contribution may come from the local thickness or composition fluctuation of GaN/AlGaN atomic layers that induce a slight change of the DA composition and consequently of the emission wavelength. Therefore, for pure GaN and $Al_{0.48}Ga_{0.52}N$ layers (assuming M_{AlGaN}=10, N_{GaN}=8 and y=0.27), ±2 MLs roughness for the total AlGaN DA was found to lead to an emission shift from 291 to 310 nm. In the same way, for the given $(GaN)_2/(AlGaN)_2$ DA, AlGaN composition fluctuating from 42 to 54% Al was found to an emission shift from 295 to 307 nm. Consequently, the width of the UV emission can be explained by thickness and/or Al-content fluctuations inside AlGaN DA.

In order to fabricate single-wire UVB LEDs, we performed electrical contacts by photolithography and e-beam evaporation. First, the wires were mechanically dispersed on a Si substrate coated with 500 nm of SiO_2. Here, as the wire diameter is typically between 1 and 3 µm, a planarization layer was required to ensure the continuity of contact between the substrate and the wire.[42] Therefore the wires were encapsulated in 2 µm-thick photoresist which would also prevent any movement of the wires during the subsequent lithography process. We then defined the metal contacts using photolithography. Finally, to simplify the technological procedure, we deposited the same metal stack (Ni 20 nm/Au 80 nm) on both n

and p sides. Based on the assumption that the mechanism responsible for the ohmic behavior of the n-contact involves the formation of a heavily n-doped layer at the interface, the electrical injection is probably much easier on the n-side as the wire core is metallic ([Si] $\sim 10^{20}$ cm^{-3}).

Two p-contacts were used to compare electrical properties of the wire-μLED: one was situated on the wire-top zone and the other below (i.e., exclusively on the m-plane DA). Figure 4a) shows the connected wire after the complete process. The I-V curves of the connected wire plotted in Figure 4b) confirm the diode rectifying behavior for the two contacts with a threshold voltage above 5 V. No leakage current from the n-GaN wire and p-GaN shell overlap was detected.[35] Special features in I-V curves were observed using log scale, as plotted in the inset of Figure 4b). The inflection point was measured near 5 V for both contacts which can be attributed to two diodes connected in parallel. This behavior has already been reported in the literature for core-shell InGaN QWs grown on microwires, related to two electrical paths from c-axis and m-axis p-n junctions.[43] In our case, the contribution from axial active zone is excluded because this behavior was found to exist even with n-p1 contact. Therefore, we believe that this feature originated from an additional GaN p-n junction formed within the cracks which are shown in Figure 2a). The schematic given in Figure 5c) illustrates current paths along single wire considering two parallel diodes. Due to the lower bandgap and higher doping of the GaN p-n through the crack, the current flows through the cracks at low bias. However, this parallel p-n junction was current limited due to reduced conduction area from the cracks. Consequently, the I-V was dominated by the AlGaN-based core-shell n-p junction at a higher bias.

Electroluminescence (EL) spectra at the same electrical power (10.8 mW) for n-p1 and n-p2 contacts are shown in Figure 5a). Two contributions with various intensity are distinguishable

from both EL spectra: the 380-nm band defect emission or so called "violet band" (VB) attributed to the emission of DAP in the p-AlGaN/GaN layer[44]; and the 310-nm emission ascribed to the AlGaN DA active region for which the emission wavelength was found to match CL observations. EL measurements were performed with a pulsed bias with a duty cycle of 1% at 10 kHz to limit the influence of Joule heating under high injection.

The EL spectrum measured with n-p1 contact exhibited degraded emission properties with concomitant higher VB intensity and lower DA emission in comparison of the n-p2 contact. This observation matches CL measurements in which the brighter intensity from AlGaN DA was measured at the top part of microwires (see Figure 3b)). Therefore, we then focused on the EL characterization on the p2 electrical contact. A voltage-dependent study was carried out using 10-16 V applied voltage. The corresponding spectra plotted in Figure 5b) were found to exhibit the same two contributions. It is interesting to note that the DA emission becomes noticeably dominant at 16 V. This feature fits well with the model of two diodes in parallel. At low injection (10 V), the emission was dominated by recombination through defects in the p-n GaN junction in the crack region, resulting in bright VB emission. At 16 V, the contribution from VB was found to saturate and the electroluminescence mainly originated from DA. We suspect that VB may also come from the emission of DAP in p-AlGaN/GaN layers due to asymmetric space charge region (SCR). In fact, acceptor concentration in p-AlGaN is assumed to be negligible with respect to donor concentration in n-AlGaN ($N_D \approx 10^{19}$ cm^3 vs $N_A \approx 10^{16}$-10^{17} cm^3). In this case, the width of SCR noted W was found to expand in the p side and is given by:

$$W \approx \sqrt{\frac{2\varepsilon_0 \varepsilon_r V_{Bi}}{eN_A}}$$

where ε_0 is the vacuum permittivity, ε_r the relative permittivity, e the electron charge, N_A concentration of acceptors atoms and V_{Bi} the built-in potential. Assuming $Al_{0.6}Ga_{0.4}N$ p-n

junction, V_{Bi}≈5 eV, ε_r≈ 9.2[45] and N_A≈10^{16}-10^{17} cm^3, W is found to approximately vary between 250 and 700 nm which is superior to total p-shell layers (≈50 nm). Indeed, the VB emission may come from DAP emission from p-AlGaN/GaN at lowest bias. Figure 5c) highlights DA and VB intensity variation for n-p1 and n-p2 contacts within a 1-10.8 mW electrical power range. For the n-p1 contact, the VB intensity increased with electrical power then saturated at the approximately 3x10^4 value while the DA contribution increased in the full electrical power range. Nevertheless, its intensity remained much lower than the VB intensity for the whole power range. For the n-p2 contact, the VB intensity increased with power reaching the approximately same 3x10^4 value which was then followed by a significant decrease. The DA emission exhibits a linear increase with power since the intensity is ten times higher at 10.8 mW compared to 1 mW. Considering this behavior, negligible VB contribution is expected at higher electrical power (> 10.8 mW).

In conclusion, embedded AlGaN DA in GaN/AlGaN p-n junction was successfully grown on m-facets of GaN microwires. HR-TEM measurements confirmed thickness homogeneity and sharp interfaces for the $(GaN)_2/(AlGaN)_2$ DA along the wires. The AlGaN-bulk like behavior was confirmed using spot mode CL measurements at 5 K and the multiple spectral contributions were attributed to thickness and/or composition fluctuation of DA. Single-wire LED was processed exhibiting a diode-like rectifying I-V behavior with EL emission at room temperature. At high voltage, AlGaN DA emits at 310 nm with significant EL intensity. This study demonstrates the high growth control by MOVPE allowing DA to be designed. This work paves the way for novel UV designs for non-polar UV LEDs and µLED based on AlGaN digital alloy heterostructures.

See the supplementary material for HAADF-STEM and TEM observations of the core-shell DA near a crack.

This work was financially supported by the Program Initiatives de Recherche Stratégiques (IRS) of IDEX Université Grenoble Alpes (ANR-15-IDEX-0002). This research was also funded by the French National Research Agency in the framework of **the program ANR-22-CE51-0032-01.** The authors thank J. Dussaud for his work on the MOVPE setup.

References

[1] W. Sun, C.-K. Tan, and N. Tansu, Sci. Rep. **7**, 11826 (2017).
[2] D.G. Ebling, L. Kirste, K.W. Benz, N. Teofilov, K. Thonke, and R. Sauer, J. Cryst. Growth 5 (2001).
[3] W. Sun, C.-K. Tan, and N. Tansu, Sci. Rep. **7**, 6671 (2017).
[4] M. Benamara, L. Kirste, M. Albrecht, K.W. Benz, and H.P. Strunk, Appl. Phys. Lett. **82**, 547 (2003).
[5] E. Iliopoulos, K.F. Ludwig, T.D. Moustakas, and S.N.G. Chu, Appl. Phys. Lett. **78**, 463 (2001).
[6] S.A. Nikishin, M. Holtz, and H. Temkin, Jpn. J. Appl. Phys. **44**, 7221 (2005).
[7] S. Adhikari, O.L.C. Lem, F. Kremer, K. Vora, F. Brink, M. Lysevych, H.H. Tan, and C. Jagadish, Nano Res. **15**, 7670 (2022).
[8] H. Kobayashi, S. Ichikawa, M. Funato, and Y. Kawakami, Adv. Opt. Mater. **7**, 1900860 (2019).
[9] N. Gao, X. Feng, S. Lu, W. Lin, Q. Zhuang, H. Chen, K. Huang, S. Li, and J. Kang, Cryst. Growth Des. **19**, 1720 (2019).
[10] D.N. Nath, Z.C. Yang, C.-Y. Lee, P.S. Park, Y.-R. Wu, and S. Rajan, Appl. Phys. Lett. **103**, 022102 (2013).
[11] D. Wang, Z. Chen, J. Su, T. Wang, B. Zhang, X. Rong, P. Wang, W. Tan, S. Guo, J. Zhang, B. Shen, and X. Wang, Adv. Funct. Mater. **31**, 2007216 (2021).
[12] J. Yun, K. Choi, K. Mathur, V. Kuryatkov, B. Borisov, G. Kipshidze, S. Nikishin, and H. Temkin, IEEE Electron Device Lett. **27**, 22 (2006).
[13] M.A. Khan, N. Maeda, J. Yun, M. Jo, Y. Yamada, and H. Hirayama, Sci. Rep. **12**, 2591 (2022).
[14] M. Shatalov, W. Sun, A. Lunev, X. Hu, A. Dobrinsky, Y. Bilenko, J. Yang, M. Shur, R. Gaska, C. Moe, G. Garrett, and M. Wraback, Appl. Phys. Express **5**, 082101 (2012).
[15] T. Takano, T. Mino, J. Sakai, N. Noguchi, K. Tsubaki, and H. Hirayama, Appl. Phys. Express **10**, 031002 (2017).
[16] M. Kneissl, T.-Y. Seong, J. Han, and H. Amano, Nat. Photonics **13**, 233 (2019).
[17] F. Mireles and S.E. Ulloa, Phys. Rev. B **58**, 3879 (1998).
[18] P. Pampili and P.J. Parbrook, Mater. Sci. Semicond. Process. **62**, 180 (2017).
[19] Y. Taniyasu, M. Kasu, and T. Makimoto, Nature **441**, 325 (2006).
[20] P. Kozodoy, M. Hansen, S.P. DenBaars, and U.K. Mishra, Appl. Phys. Lett. **74**, 3681 (1999).
[21] A. Hirano, Y. Nagasawa, M. Ippommatsu, H. Sako, A. Hashimoto, R. Sugie, Y. Honda, H. Amano, K. Kojima, and S.F. Chichibu, Appl. Phys. Express **15**, 075505 (2022).
[22] M. Nami, A. Rashidi, M. Monavarian, S. Mishkat-Ul-Masabih, Ashwin.K. Rishinaramangalam, S.R.J. Brueck, and D. Feezell, ACS Photonics **6**, 1618 (2019).
[23] R. Koester, D. Sager, W.-A. Quitsch, O. Pfingsten, A. Poloczek, S. Blumenthal, G. Keller, W. Prost, G. Bacher, and F.-J. Tegude, Nano Lett. **15**, 2318 (2015).
[24] M. Leroux, N. Grandjean, M. Laügt, J. Massies, B. Gil, P. Lefebvre, and P. Bigenwald, Phys. Rev. B **58**, R13371 (1998).
[25] J. Kim, U. Choi, J. Pyeon, B. So, and O. Nam, Sci. Rep. **8**, 935 (2018).
[26] P.-M. Coulon, G. Kusch, R.W. Martin, and P.A. Shields, ACS Appl. Mater. Interfaces **10**, 33441 (2018).
[27] P.-M. Coulon, G. Kusch, P. Fletcher, P. Chausse, R. Martin, and P. Shields, Materials **11**, 1140 (2018).
[28] H. Spende, C. Margenfeld, and A. Waag, ACS Photonics **9**, 1594 (2022).
[29] C. Durand, J.-F. Carlin, C. Bougerol, B. Gayral, D. Salomon, J.-P. Barnes, J. Eymery, R. Butté,

and N. Grandjean, Nano Lett. **17**, 3347 (2017).
[30] S. Finot, V. Grenier, V. Zubialevich, C. Bougerol, P. Pampili, J. Eymery, P.J. Parbrook, C. Durand, and G. Jacopin, Appl. Phys. Lett. **117**, 221105 (2020).
[31] C. Durand, C. Bougerol, J.-F. Carlin, G. Rossbach, F. Godel, J. Eymery, P.-H. Jouneau, A. Mukhtarova, R. Butté, and N. Grandjean, ACS Photonics **1**, 38 (2014).
[32] V. Grenier, S. Finot, G. Jacopin, C. Bougerol, E. Robin, N. Mollard, B. Gayral, E. Monroy, J. Eymery, and C. Durand, ACS Appl. Mater. Interfaces **12**, 44007 (2020).
[33] Y. Ra, S. Kang, and C. Lee, Adv. Opt. Mater. **6**, 1701391 (2018).
[34] R. Koester, J.S. Hwang, C. Durand, D. Le Si Dang, and J. Eymery, Nanotechnology **21**, 015602 (2010).
[35] P. Tchoulfian, F. Donatini, F. Levy, B. Amstatt, P. Ferret, and J. Pernot, Appl. Phys. Lett. **102**, 122116 (2013).
[36] P. Tchoulfian, F. Donatini, F. Levy, A. Dussaigne, P. Ferret, and J. Pernot, Nano Lett. **14**, 3491 (2014).
[37] A. Kapoor, S. Finot, V. Grenier, E. Robin, C. Bougerol, J. Bleuse, G. Jacopin, J. Eymery, and C. Durand, ACS Appl. Mater. Interfaces **12**, 19092 (2020).
[38] V. Grenier, S. Finot, B. Gayral, C. Bougerol, G. Jacopin, J. Eymery, and C. Durand, Cryst. Growth Des. **21**, 6504 (2021).
[39] M.A. Khan, J.P. Bermundo, Y. Ishikawa, H. Ikenoue, S. Fujikawa, E. Matsuura, Y. Kashima, N. Maeda, M. Jo, and H. Hirayama, Nanotechnology **32**, 055702 (2021).
[40] S. Einfeldt, V. Kirchner, H. Heinke, M. Dießelberg, S. Figge, K. Vogeler, and D. Hommel, J. Appl. Phys. **88**, 7029 (2000).
[41] S.R. Lee, A.F. Wright, M.H. Crawford, G.A. Petersen, J. Han, and R.M. Biefeld, Appl. Phys. Lett. **74**, 3344 (1999).
[42] P. Tchoulfian, F. Donatini, F. Levy, B. Amstatt, A. Dussaigne, P. Ferret, E. Bustarret, and J. Pernot, Appl. Phys. Lett. **103**, 202101 (2013).
[43] G. Jacopin, A. De Luna Bugallo, P. Lavenus, L. Rigutti, F.H. Julien, L.F. Zagonel, M. Kociak, C. Durand, D. Salomon, X.J. Chen, J. Eymery, and M. Tchernycheva, Appl. Phys. Express **5**, 014101 (2012).
[44] V. Grenier, S. Finot, L. Valera, J. Eymery, G. Jacopin, and C. Durand, Appl. Phys. Lett. **121**, 131102 (2022).
[45] O. Ambacher, J. Smart, J.R. Shealy, N.G. Weimann, K. Chu, M. Murphy, W.J. Schaff, L.F. Eastman, R. Dimitrov, L. Wittmer, M. Stutzmann, W. Rieger, and J. Hilsenbeck, J. Appl. Phys. **85**, 3222 (1999).

Figure caption

Figure 1: Schematic of GaN microwire-based core-shell structure with 5x $(GaN)_2/(AlGaN)_2$ active area integrated in the middle of n-GaN/n-AlGaN/p-AlGaN/p-GaN junction.

Figure 2: (a) HAADF-STEM images of longitudinal cross section of core-shell GaN/AlGaN microwire. (b, c, d) Off-axis HR-TEM images of active zone along $[10\bar{1}0]$ axis with 10°-tilt compared to $[11\bar{2}0]$ axis zone with different magnifications.

Figure 3: (a) SEM image of typical wire with rainbow-colored dots and (b) the corresponding normalized CL spectra in spot mode measured at 5K. Various contributions are highlighted using dotted lines and arrows.

Figure 4: (a) SEM image of contacted single microwire with n, p1 and p2 contacts. (b) Room temperature IV measurements of contacted microwire between n-p1 and n-p2 contacts. IV curves in log scale are plotted in inset. (c) Schematic of current path along single wire considering two parallel diodes.

Figure 5: (a) Room temperature EL spectra of microwire at 10.8 mW electrical power for both n-p1 and n-p2 contacts. (b) Voltage dependent study (10-16 V) of microwire between n and p2 contacts. (c) Evolution of maximal intensity of both VB and AlGaN DA contributions in function of electrical power plotted for n-p1 and n-p2 contacts.

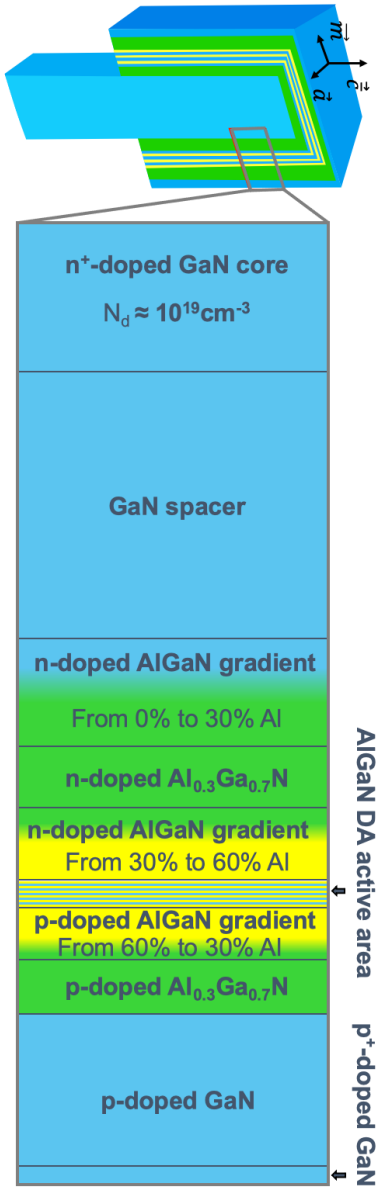

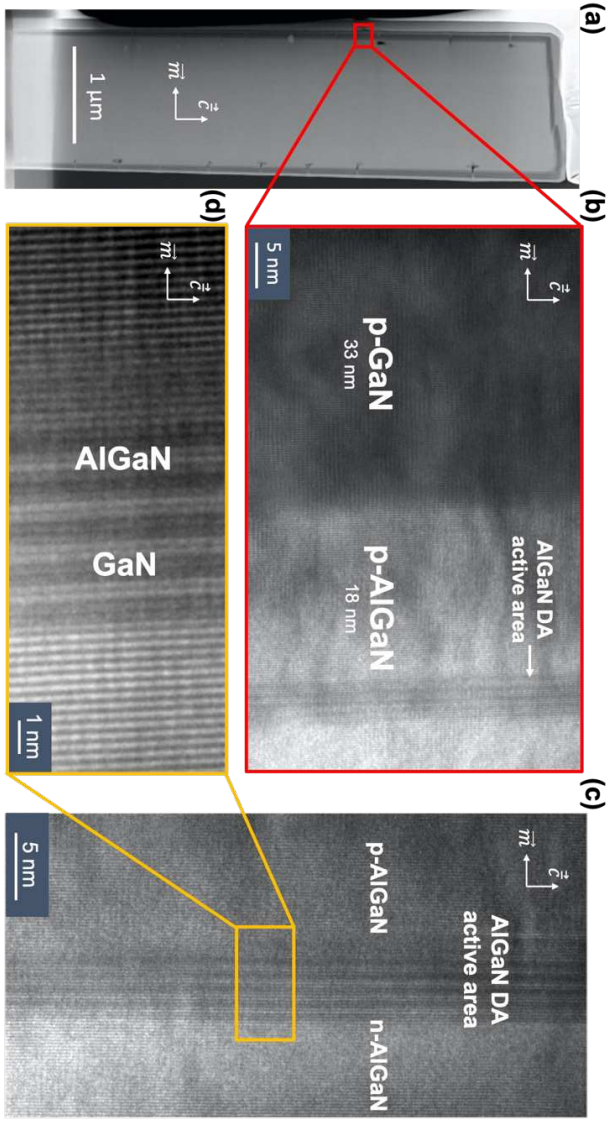

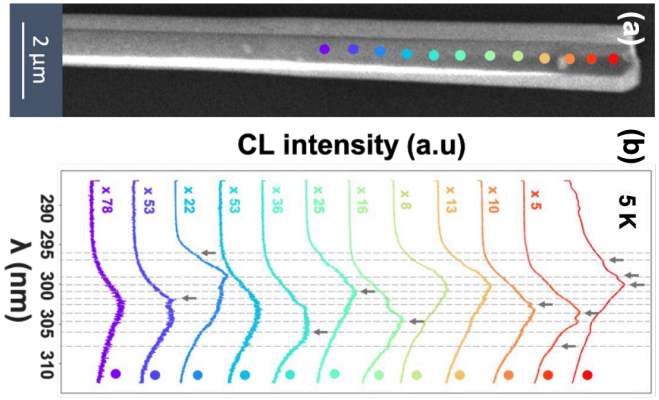

PLEASE CITE THIS ARTICLE AS DOI: 10.1063/5.0141568

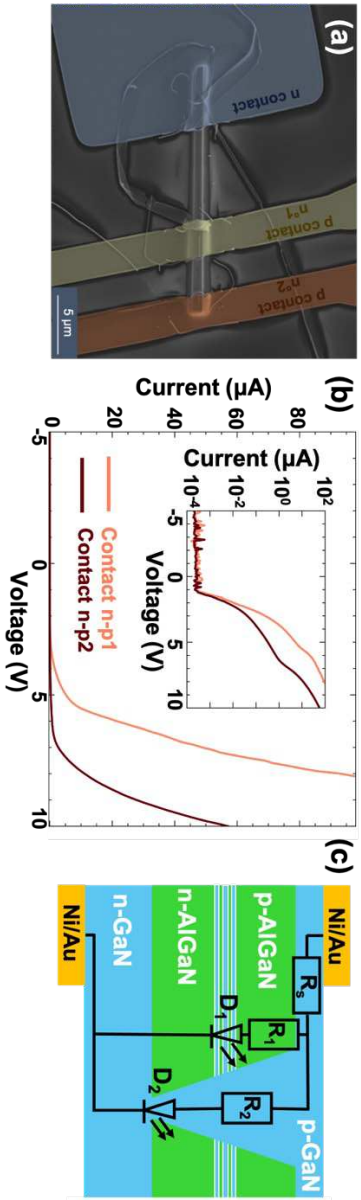

PLEASE CITE THIS ARTICLE AS DOI: 10.1063/5.0141568